Effects of O_2 plasma and UV-O_3 assisted surface activation on high sensitivity metal oxide functionalized multi-walled carbon nanotube CH_4 sensors

Md Tanim Humayun,[1] Michela Sainato,[1] Ralu Divan,[2] Richard A. Rosenberg,[3] Alvaro Sahagun,[1] Lara Gundel,[4] Paul A. Solomon,[5] and Igor Paprotny[1, a)]

[1)] *Department of Electrical and Computer Engineering, University of Illinois at Chicago, Chicago, Il 60607*

[2)] *Center for Nanoscale Materials, Argonne National Laboratory, Argonne Il 60439*

[3)] *Advanced Photon Source, Argonne National Laboratory, Argonne Il 60439*

[4)] *Lawrence Berkeley National Laboratory, Berkeley, CA 94720*

[5)] *U. S. Environmental Protection Agency, Las Vegas, NV 89199*

(Dated: 23 August 2017)

We present a comparative analysis of UV-O_3 (UVO) and O_2 plasma-based surface activation processes of multi-walled carbon nanotubes (MWCNTs) enabling highly effective functionalization with metal oxide nanocrystals (MONCs). Experimental results from transmission electron microscopy (TEM), scanning electron microscopy (SEM), X-ray photoelectron spectroscopy (XPS), and Raman spectroscopy show that by forming COOH (carboxyl), C-OH (hydroxyl), and C=O (carbonyl) groups on the MWCNT surface that act as active nucleation sites, O_2 plasma and UVO-based dry pre-treatment techniques greatly enhance the affinity between MWCNT surface and the functionalizing MONCs. MONCs, such as ZnO and SnO_2, deposited by atomic layer deposition (ALD) technique, were implemented as the functionalizing material following UVO and O_2 plasma activation of MWCNTs. A comparative study on the relative resistance changes of O_2 plasma and UVO activated MWCNT functionalized with MONC in the presence of 10 ppm methane (CH_4) in air, is presented as well.

Keywords: Gas sensor, Carbon Nanotube, Methane

I. INTRODUCTION

Methane (CH_4) gas has a 100 year global warming impact factor of 24-36 compared to CO_2[1]. With the emergence of the U.S. as the world's leading producer of natural gas, it is important to enable widespread monitoring of CH_4 emission from natural gas infrastructures. Metal oxide chemoresistive sensors are widely used to sense CH_4[2–4]. Continuous heating is necessary for these sensors to initiate the surface chemisorption of O_2, a prerequisite to detect CH_4, often requiring 100s of milliwatts (mWs) of power[2–5]. Carbon Nanotube (CNT)-based chemoresistor sensors have demonstrated ppm levels of gas sensing at room temperature, with power consumption of only few mWs[5]. This is a direct outcome of CNT's high surface-to-volume ratio and outstanding modulation of electrical conductance during interaction with gas species. However, functionalizing particles (ranging from metal[5], metal oxides[6], polymer coating[7] to biomolecules[8]) must be deposited uniformly on the surface of pristine carbon nanotubes in order to enable effective and reversible electrical modulation in the presence of target gas species. Unfortunately, in general, the surface of CNTs show poor affinity with the functionalizing materials[9–13]. Consequently, before applying the functionalization materials, *activation* of the inert graphitic surface of the CNTs is necessary[9–11].

We present here a comparative analysis of novel UV-O_3 (UVO) and O_2 plasma-based surface activation processes, that enable highly effective functionalization of multi-walled carbon nanotubes (MWCNTs) with metal oxide nanocrystals (MONCs). O_2 plasma and UVO-based dry surface activation techniques have not been applied in CNT-based CH_4 chemoresistor sensors before[5,14,15]. Weak affinity among the CNT surface and the functionalizing nano-partcles, resulting from the absence of surface activation, may greatly affect the sensor's reversible response to low ppm methane concentrations. Experimental results from transmission electron microscopy (TEM), scanning electron microscopy (SEM), X-ray photoelectron spectroscopy (XPS), and Raman spectroscopy show that by forming COOH (carboxyl), C-OH (hydroxyl), and C=O (carbonyl) groups on the MWCNT surface, that act as active nucleation sites, O_2 plasma and UVO-based dry activation techniques greatly enhance the affinity between MWCNT surface and the functionalizing MONCs. We have implemented MONCs such as ZnO and SnO_2 as the functionalizing material following UVO and O_2 plasma activation of MWCNTs. MONCs were deposited by atomic layer deposition (ALD) technique[16–18].These metal oxides are less expensive than previously reported functionalizing materials (e.g. Pd) used in CNT-based CH_4 sensors[5,6]. Electron transport is energetically favorable in the ZnO-MWCNT or SnO_2-MWCNT junctions whereas Pd forms a significant Schottky barrier with bare CNTs[5,6,19,20]. A comparative study on the relative resistance changes of O_2 plasma and UVO activated MONC functionalized MWCNT chemoresistive sensors, under the presence of 10 ppm CH_4 in air, is presented. After CH_4 exposure

[a)] Electronic mail: paprotny@uic.edu

the sensors were recovered to baseline resistance by N_2 purging. An analysis of the effect of relative humidity (RH) on the sensor response is also presented, showing superior performance to other previously reported CNT CH_4 sensors.

Traditionally, the surface of bare CNTs is activated by exposing it to high temperature vapors[10] and/or using wet chemistry[11]. Depending on temperature and air-exposure, the high-temperature may actually destroy or excessively damage the CNTs[10]. Acid treatments used in wet chemistry can considerably reduce the mechanical and electric performance of the tubes by introducing large numbers of defects[21]. Wet chemistry also involves additional steps, such as dissolution, sonication, mixing, and drying, which often causes undesirable agglomeration of treated CNTs[10].

To increase the efficiency of CNT functionalization, two alternative dry activation processes have been proposed: (a) gas plasma[9–11], and (b) UVO treatment[22].

Due to the interaction of surface C atoms with active O atoms during O_2 plasma or UVO activation, and subsequent exposure to atmosphere, chemical groups such as COOH (carboxyl), C=O (carbonyl), C-OH (hydroxyl) and C-O-C (ether) are formed on the MWCNT surface[11–13,23,24]. These groups act as active sites for the nucleation of MONCs[11–13,22]. Both the O_2 plasma and UVO exposure have no effect on the aspect ratio (i.e. length to diameter ratio) of the MWCNTs[21].

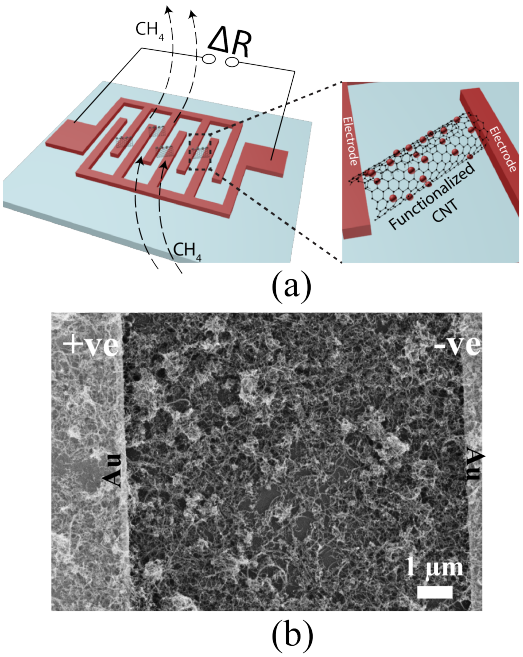

FIG. 1. (Color online)(a) The concept of MONC-MWCNT CH_4 chemoresitive sensors. The sensor acts as a resistor that changes resistance when exposed to CH_4.(b) SEM image of ZnO functionalized MWCNTs confined between two Au electrodes.

II. EXPERIMENT

A. Sensor Fabrication

We fabricated surface activated MONCs (ZnO or SnO_2) functionalized MWCNT chemoresistive CH_4 sensors using the following fabrication steps: (1) lift-off based photolithography, (2) O_2 plasma or UVO based surface activation, and (3) ALD based fuctionalization. The sensor concept is illustrated on Fig. 1a. Fig. 1b shows an SEM image of the sensor where functionalized MWCNTs can be seen deposited between a pair of Au electrodes.

Interdigitated Au electrodes were fabricated by photolithography. Details on the fabrication process can be found elsewhere[25].

MWCNT (98 % pure) with an average diameter of 12 nm, average lengths of 10 μm and a specific surface area of 220 m^2/g was purchased from Sigma Aldrich. Using a micro-syringe, an aliquot of 50 μL from a 1 g/50 mL solution of MWCNT-ethanol was deposited on an active area of 1 mm^2 on the fabricated Au electrodes. It was followed by baking the devices at 75 °C to remove the ethanol and improve adhesion.

The deposited MWCNTs were O_2 plasma activated in a reactive ion etching (RIE) chamber (March plasma CS-1701). The base pressure of the plasma chamber was almost 40 mTorr. O_2 was introduced at a flow rate of 20 standard cubic centimeter per minute (sccm) while the pressure was maintained at 160 mTorr during the process. O_2 plasma was generated by applying a radio frequency (RF) of 13.56 MHz with a power of 100 watts. The duration of the plasma treatment was 5 min. A UVO cleaner (Nanonex Ultra 100) was used for the UVO treatment of the MWCNT surface where a 185 nm UV was radiated to atmosphere for generating O_3 and activating the MWCNT surface. The process duration was 20 min.

Using diethylzinc ($(C_2H_5)_2Zn$) as a precursor, ALD of ZnO on the surface activated MWCNTs was performed with an Arradiance Gemstar ALD tool (Details can be found here[25]).

ALD was also used to deposit SnO_2 NCs on to the surface activated MWCNTs. The growth was done using an Ultratech Savannah S200 with tetrakis (dimethylamino)tin(IV) as a pre-cursor (Details can be found here[26]).

B. TEM sample preparation and imaging

Holey carbon film on Cu grids was used to prepare the TEM sample. Using a micro-syringe, an aliquot of 50 μL from a 1 mg/50 μL solution of MWCNT-ethanol solution was deposited on the TEM grid. It was followed by baking the devices at 75 °C to remove the ethanol

and improve adhesion. MWCNTs were surface activated in a similar manner described in Section II A (5 min O_2 plasma or 20 min UVO).

ALD of ZnO or SnO_2 was performed following the similar approach described in Sub-section II A.

A JEOL 2100F TEM operated at 200 kV was used to characterize atomic scale morphology and crystal quality of the MONCs deposited on MWCNT surfaces.

C. XPS sample preparation

20 nm Au were deposited on clean Si wafer using electron beam evaporation. Using a micro-syringe, an aliquot of relatively higher density solution (1 mg/1 μL) of MWCNT-ethanol was deposited on the Au-coated Si wafers. It was followed by baking the devices at 75 °C to remove the ethanol and improve adhesion. MWCNTs were surface activated in a similar manner as described in Section II A (5 min O_2 plasma or 20 min UVO).

D. Test Setup and Approach

Sensors were exposed to a 10 ppm mixture of CH_4 in synthetic air (20.81% of O_2 and 79.19 % of N_2; prepared by Praxair Inc.). The flow rate was maintained at 0.94 L/min with a residence time of 4.5 min inside the plastic test chamber (details elsewhere[25]). After the CH_4 exposure, the sensors were flushed with N_2 (same flow rate as CH_4, 0.94 L/min). The electrical signal obtained from the sensors were recorded using a custom interface circuit connected to a computer. A HOBO temperature and RH sensor was used to continuously monitor and record the RH and temperature inside the plastic test chamber during the test.

III. RESULTS AND DISCUSSION

A. Sample Characterization

High resolution XPS ($h\nu$=650 eV) was carried out using beamline 4-ID-C at the Advanced Photon Source (APS), Argonne National Laboratory. MWCNTs were deposited on gold-covered silicon substrates and subsequently activated by O_2 plasma or UVO. Binding energies were calibrated to the Au 4f binding energy of 84.0 eV. Quantification was performed using XPS data analysis software CasaXPS. Fig. 2 shows the C 1s and O 1s peaks originating from pristine (a, d), 5 min O_2 plasma activated (b, e) and 20 min UVO activated MWCNT (c, f). The assignments of the C 1s and O 1s components were based on reported spectra containing specific oxygen functional groups[24,27–29]. The measured spectra were fitted to a function having 70% Gaussian and 30% Lorentzian character, after performing a Shirley background correction. The C1 component centered at 284.3 eV represents the sp^2 graphitic component. The components at 285.4 eV, 286.5 eV, 287.7 eV and 289.1 eV (C2 up to C5) were assigned to C atoms forming C-OH, C-O-C, C=O and COOH functional groups, respectively[24,27–29]; the components at 531.1 eV (O1), 532.2 eV (O2), 533.5 eV (O3), and 534.7 eV (O4) were assigned to O atoms forming C=O, C-OH, C-O-C, and H_2O, respectively[24,27–29].

The normalized peak areas (NPA) of various components of C 1s and O 1s spectra were calculated with respect to the area of their respective C1 component (sp^2) (Table I). Comparison among the NPA of C5 (COOH group) in several samples suggests that COOH is the primary chemical group created by the surface activation process. The NPA of C-OH components (C2 and O2) are significantly larger in the surface activated sample compared to the pristine sample, suggesting a strong presence of C-OH in the surface activated MWCNT as well. The NPA of C4 and O1, representing the C=O group, were found to be highest in the 5 min plasma activated MWCNT, but insignificant in pristine and 20 min UVO activated MWCNT. On the other hand, the NPA of the C3 and O3, representing the C-O-C functional group, were found to be highest in the pristine MWCNT (Table I).

It is well known that active π bonds in C=C are dissociated during plasma/UVO activation and -C$^{\cdot}$ free radicals are produced[11,23,24]. Subsequently, -C$^{\cdot}$ free radicals are oxidized by active O atoms present in O_2 plasma and UVO, resulting into C-O and C=O bonds[23,24]. After prolonged interaction with plasma/UVO, C=O is further oxidized and O-C=O is formed[23,24]. Due to atmospheric exposure, C-O and O-C=O stabilize by reacting with ambient H_2O and generate C-OH and COOH, respectively[23]. This is the probable cause of the strong presence of COH and COOH groups in our plasma/UVO activated MWCNTs. Surface C atoms of pristine MWCNT react with atmospheric H_2O to create C-O, a probable cause of presence of C-O-C group in pristine MWCNT[24].

In summary, XPS results corroborate that the surface activation process produces the COOH functional group along with C-OH and C=O. In later steps these groups help with nucleating the functionalizing MONCs on the surface of the MWCNTs.

The TEM micrographs show that MONCs are not visible on the surface of the non-activated but ALD processed MWCNTs (Fig. 3a). Uniform deposition of ZnO-MONCs was found on the surface of the activated MWCNTs (Fig. 3b). The clearly visible lattice fringes on the higher resolution TEM (HRTEM) image in Fig. 3d illustrates the wurtzite structure of the ZnO MONC and its good crystalline quality. The interplanar spacings of 2.8 Å, 2.68 Å and 2.48 Å correspond to the <100>, <002> and <101> planes of ZnO, respectively[30]. The HRTEM image in Fig. 3c shows the atomic scale morphology of rutile SnO_2 MONCs deposited on the MWCNT surface.

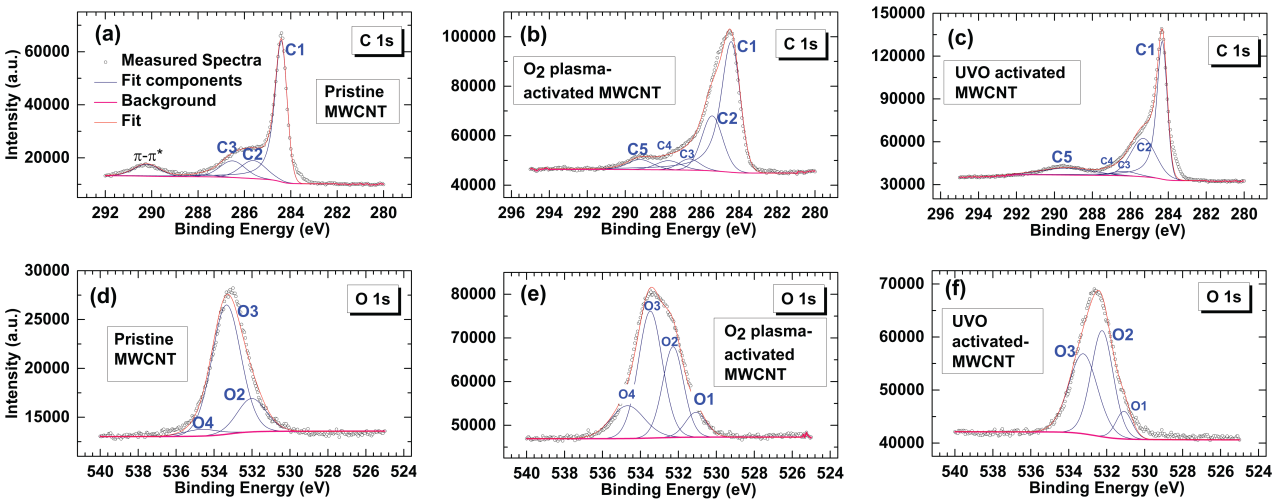

FIG. 2. (Color online)(a)-(c): C 1s XPS peaks: (a) pristine MWCNTs (b) 5 min O_2 plasma activated MWCNTs, and (c) 20 min UVO activated MWCNTs. (d)-(f): O 1s XPS peaks: (d) pristine MWCNTs (e) 5 min O_2 plasma activated MWCNTs, and (f) 20 min UVO activated MWCNTs.

TABLE I. Comparison between normalized peak areas (NPA; with respect to C1) of C 1s (C2 to C5) and O 1s (O1 to O3) peak components in pristine, plasma activated, and UVO activated MWCNT samples.

Peak Component	Location (eV)	Functional Group	**NPA**		
			Pristine MWCNT	Plasma Activated MWCNT	UVO Activated MWCNT
C2	285.4	C-OH	0.29	0.50	0.73
C3	286.5	C-O-C	0.26	0.10	0.08
C4	287.7	C=O	0.03	0.10	0.02
C5	289.1	COOH	not present	0.11	0.26
O1	531.1	C=O	0.02	0.13	0.09
O2	532.2	C-OH	0.20	0.47	0.48
O3	533.5	C-O-C	0.77	0.76	0.47

The interplanar spacings of 2.6 Å and 3.3 Å correspond to <101> and <110> planes of SnO_2, respectively[6]. TEM results validate the hypothesis that surface activation of the MWCNTs is essential for effective functionalization, i.e., nucleation and stronger binding of the MONCs to surfaces the MWCNTs.

Room temperature Raman spectroscopy was performed using a Renishaw Invia micro-Raman system with a 514 nm laser. Three types of ZnO ALD functionalized MWCNTs samples were used in the Raman characterization: (1) O_2 plasma activated, (2) UVO activated, and (3) non-activated, i.e., untreated. Raman spectra, illustrated in Fig. 4, reveal that after the surface activation and ALD functionalization, the D, G and G' band peaks of the MWCNTs are preserved, while additional Raman peaks originating from the ZnO NCs appeared. The characteristic Raman peaks of ZnO NCs, represented by m, n, o and p were observed only on the O_2 plasma activated samples (1) n, o and p, were observed on the UVO activated samples (2), while none of these peaks were visible on the untreated MWCNTs samples (3); consistent with the hypothesis that the ZnO NC functionalization is enhanced in surface-activated MWCNTs. The peaks described in Fig. 4b– 200.6 cm^{-1} (m), 324.25 cm^{-1} (n), 430.84 cm^{-1} (o), 569.87 cm^{-1} (p)–correspond to $2E_2^{low}$, $E_2^{high} - E_2^{low}$, E_2^{high}, A_1(LO), modes of ZnO[31,32], respectively, suggesting that surface activated samples have ZnO NCs with high crystalline quality. In addition, the characteristic ZnO Raman peaks are sharper in O_2 plasma activated MWCNTs than in UVO activated MWCNTs. The full width at half maximum (FWHM) of the A_1(LO) peak was found to be 50.5 cm^{-1} and 62.29 cm^{-1} for O_2 plasma activated and UVO activated samples, respectively, also suggesting superior crystal quality of ZnO on O_2 plasma activated MWCNTs[31]. Consequently Raman characterization results also validate the

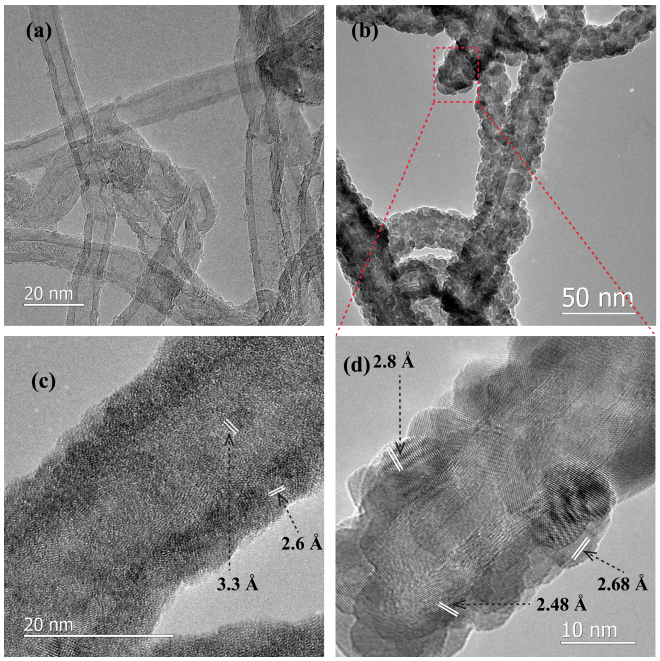

FIG. 3. (Color online)(a) The transmission electron microscopy (TEM) image of untreated but ZnO deposited MWCNTs. ZnO nanocrystals were not visible on the surface of these untreated MWCNTs. (b) Uniform distribution of atomic layer deposited ZnO nanocrystals on the UVO activated MWCNT surface. (c) High resolution TEM image of a SnO_2-MWCNT (ALD at 175 ^{0}C) sample showing interplanar spacing of 2.6 Åand 3.3 Å corresponding to $< 101 >$ and $< 110 >$ planes of SnO_2. (d) High resolution TEM image of a ZnO-MWCNT (ALD at 175 ^{0}C) sample showing interplanar spacing of 2.8 Å, 2.68 Åand 2.48 Å corresponding to $< 100 >, < 002 >$, and $< 101 >$ planes of ZnO.

hypothesis that surface activation of the MWCNTs is essential for effective functionalization, i.e., stronger nucleation and binding of the MONCs onto the MWCNTs surfaces.

The G peak represents the movement in the opposite direction of two neighboring carbon atoms in a graphitic sheet hence indicating the presence of crystalline graphitic carbon in MWCNTs[10]. While the D peak represents the defects in the curved graphite sheet, sp^3 carbon, or other impurities[33]. The I_D/I_G ratio, where I corresponds to the peak area of the Lorentzian functions, is an estimate of the relative structural defects. Our preliminary characterization suggests that due to O_2 plasma activation the relative intensity of the D-peak with respect to the G-peak (I_D/I_G ratio) of the MWCNT increases 13.5%. The results are presented in the supporting document. The probable reason for the increase in the intensity of the D-peak with respect to the G peak is the presence of reactive sites on the surface of the MWNTs created by O_2. These sites are supposed to enhance the uniform distribution of the metal oxide nanoparticles on the MWCNT surface.

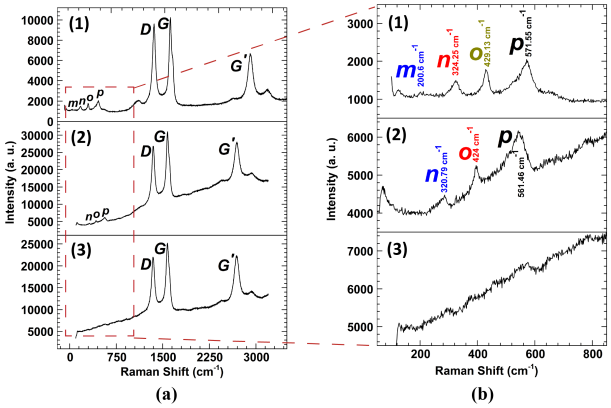

FIG. 4. (Color online)(a) Raman spectra obtained from the O_2 plasma activated ZnO functionalized MWCNT (top panel), UVO activated ZnO functionalized MWCNT (middle panel), and untreated but ZnO functionalized MWCNT (bottom panel). (b) Enlarged ZnO peaks in the range of 100 cm^{-1} to 850 cm^{-1} frequency shift.

B. Methane Sensing

Our hypothesis is that MONCs help chemisorption of methane gas molecules on the surface of the activated MWCNTs. We found that the resistance of the MONC-MWCNT sensors increases in presence of a mixture of methane in dry air. The relative resistance change has been defined as:

$$\Delta R/R = (R_{methane} - R_{air})/R_{air}$$

A series of experiments were conducted to evaluate the effect of UVO and O_2 plasma treatments on the performance of the MONC-MWCNT sensor. To decouple the sensor response to CH_4 from the interference of variable RH, the RH inside the test chamber was kept constant and monitored in real time during each test period. The relative resistance of the sensor monotonically increased at room temperature when 10 ppm CH_4 in air was introduced to the test chamber. While maintaining a constant flow rate, when the incoming gas was switched from CH_4 to N_2, the relative resistance of the sensor decreased and returned to the baseline (Fig. 5 a-c). The sensing mechanism could be elucidated from this phenomenon: the monotonic increase in the sensor's relative resistance is a result of absorption of CH_4 molecules on the MONC functionalized MWCNT surface.

Fig. 5 also corroborates the assumption that surface activation is essential for effective functionalization of the MWCNT by MONCs and for the sensor to act reversibly in the presence and absence of 10 ppm CH_4 in air. Fig. 5a and 5b show reproducible change in the relative resistance of the surface activated ZnO-MWCNT sensor during alternating exposure to CH_4 and N_2. Fig. 5c illustrates a surface activated SnO_2-MWCNT chemore-

sistor sensor alternatively exposed to CH_4 and N_2 showing similarity to ZnO-MWCNT result. No discernible signals were observed from the untreated (but ZnO NC deposited) MWCNT sensor (Fig. 5d).

At room temperature, the average relative resistance change ($\Delta R/R = (R_{methane} - R_{air})/R_{air}$) was found to be $1.91 \pm 0.98\%$ for UVO activated, and $10.5 \pm 1.01\%$ for O_2 plasma activated ZnO-MWCNT sensors. The results show that the O_2 plasma activation significantly enhances the affinity of the MONCs (in this case ZnO NCs) to the MWCNTs surface in comparison to UVO activation. This enhanced affinity causes stronger electron transport through the ZnO-MWCNT junction, i.e, a larger resistance change in the presence of CH_4 at room temperature (Fig. 5a-b). This is likely due to the better crystal quality of the ZnO NCs on O_2 plasma activated MWCNTs compared to UVO activated MWCNTs (as also indicated by the Raman results in Fig. 4).

A novel UV-based recovery technique was recently presented by our group[34]. The sensor was first exposed to 10 ppm CH_4 in air for 30 min., and without interrupting the flow of CH_4, the sensor was irradiated with a UV light until the sensor returned to its baseline resistance. No N_2 flow was used during the recovery. A recovery time of about 3 minutes was observed. The improvement in the recovery time, we believe, was due to the UV induced reduction of the desorption energy barrier of the CH_4 molecules at the sensor surface[5].

To verify the sensor response to methane, the ZnO-MWCNT sensor was tested at varying CH_4 concentrations (2 ppm, 5 ppm, and 10 ppm in dry air), at room temperature. 2 ppm and 5 ppm methane were obtained from dilution of 10 ppm methane in synthetic air. The sensors were exposed to CH_4 for 10 min (gas phase) and then to nitrogen for 10 min (desorbing phase), repeating this protocol on the entire set of experiments. The response from a representative sensor is shown on Fig. 6. The sensors were also tested for, and displayed zero cross-sensitivity to O_2. The cross-sensitivity to O_2 was determined to be insignificant comparing the sensitivity of the sensor to a variable dilution of O_2 in N_2, i.e., synthetic air (results not shown here)

The sensitivity of a semiconducting oxide gas sensor is defined as follows[5,6]:

(a) for reducing gas:

$$\Delta R/R = (R_{gas} - R_{air})/R_{air}$$

(b) for oxidizing gas:

$$\Delta R/R = (R_{air} - R_{gas})/R_{gas}$$

where R_{air} is the resistance of the sensor in air, R_{gas} is the resistance of the sensor in presence of gas and air.

We found that the resistance of the MONC-MWCNT sensors changes in presence of a mixture of methane in air. The change in resistance is in accordance with the change in resistance of SnO_2-MWCNT nano-hybrid reported by Ganhua Lu et. al.[6], where they show the resistance of SnO_2-MWCNT nano-hybrid decreases in presence of oxidizing NO_2. A possible sensing mechanism has been reported by Ganhua Lu et. al.[6]. Target molecules, in this case NO_2, get directly adsorbed onto the SnO_2-MWCNT surface, facilitate electron transfer and change the electrical conductivity of the hybrid nanostructure.

One can find references that describe electronic properties of MWCNTs as metallic[35,36] or semiconductive[6,37–39]. However, ZnO and SnO_2 are widely known as n-type material[6,32], and the presence of a reducing gas, such as CH_4, alters their charge concentration, resulting in a change in the resistance of the MONC-MWCNT conglomerate, which was observed experimentally.

A deeper investigation on the methane-functionalized CNT surface interaction is in order, however this is beyond the scope of this paper. Furthermore, we are currently conducting experiments to study the electronic property of surface pre-treated metal oxide nanocrystal functionalized MWCNTs, which will help us understand their methane gas sensing mechanism more thoroughly.

Understanding the effect of relative humidity (RH) is important to estimate the outdoor performance of microfabricated gas sensors. To examine the effect of relative humidity (RH) on sensor performance, the change in the baseline relative resistance of the surface activated ZnO-MWCNT sensors was measured at room temperature due to a change in RH. Humidity was provided by a controlled flow of moist air (flow rate 0.94 L/min) into a plastic test chamber (residence time 4.5 min). The baseline relative resistance of the sensor increased by about 4% as the RH was increased from 10% to 91% and returned back to the original baseline once the RH was reduced back to 10%. This suggests a strong electron transfer between the MONC functionalized MWCNTs and water molecules (Fig. 7). Our ongoing research involves fabricating a network of MWCNTs selectively functionalized with various metal oxide nanoparticles with different sets of sensitivities to CH_4 and H_2O. By deconvoluting the constructive/destructive interference in various RH levels, the RH contribution can be effectively determined and separated from the device's response to CH_4 .

We explored the relative resistance change for 10 ppm methane at two different RH levels[26]. While exposing the SnO_2-MWCNT sensor to 10 ppm of CH_4 in dry air at the higher RH (approximately 70%), a monotonic resistance increment was observed which was similar to the low RH tests where RH was held constant at 5%, as seen in Fig.8. The sensor also equilibrated to its original response in a similar fashion when the chamber was purged with N_2. The response to CH_4 and signal-to-noise ratio reduced in comparison to those at lower RH, which we believe was a result of adsorbed H_2O molecules on the SnO_2-MWCNT sensor. Although the sensor showed reduced response it was still capable of detecting 10 ppm CH_4 in air at 70% RH. We observed a monotonic increase in the sensor resistance while it was exposed to CH_4 at low and high RH, as well as monotonic decrease (return to baseline)

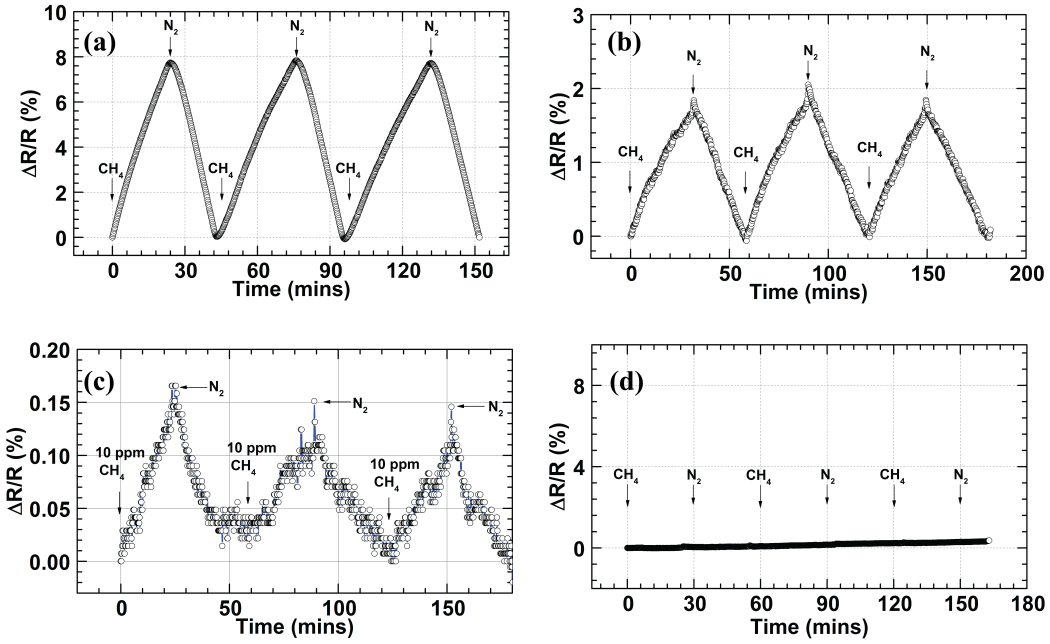

FIG. 5. Comparison of the dynamic sensor response ($\Delta R/R = (R_{methane} - R_{air})/R_{air}$) of MONC-MWCNT sensors to 10 ppm CH_4 in dry air, followed by flushing with N_2 for sensor recovery. Each section of the figure shows $\Delta R/R$ for: (a) O_2 plasma treated ZnO functionalized, (b) a UVO treated ZnO functionalized, (c) a UVO treated SnO_2 functionalized, and (d) an untreated but ZnO deposited MWCNT sensor.

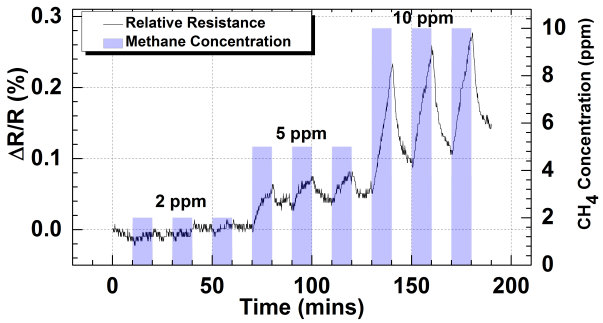

FIG. 6. (Color online) Relative resistance change of an O_2 plasma activated ZnO functionalized MWCNT sensor under exposure to 2 ppm, 5 ppm and 10 ppm of CH_4 in dry air mixture at room temperature. RH was kept constant at 2% during the experiment. A different metal electrode/CNT configuration was used resulting in smaller relative resistance change compared to 5a.

when the CH_4 was purged with N_2 (Fig. 8). The sensor behavior is similar at both low and high humidity, although the sensitivity is reduced at high RH. This is likely the result of absorbed H_2O molecules on the sensor surface. Water molecules are found to behave as electron donor on the surface of carbon nanotubes[40–42]. It was reported that a hydrogen-bonded water monolayer forms around the nanotube at fully water covered condition[40]. Na et al.[40] presented the change in electrical resistance as a function of relative humidity which agrees with the result presented in Fig. 8 i.e., a decrease in the relative change of resistance (ΔR) at high RH condition. This can be attributed to electron donation by the H_2O molecules on the sensor surface[40,42]. Our ongoing work focuses on studying the response of the MONC-MWCNT sensor at a fixed ppm methane for multiple RH%.

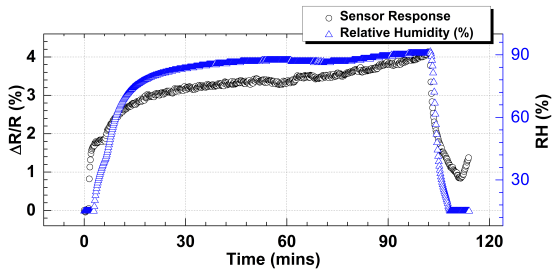

FIG. 7. (Color online) Relative resistance change ($\Delta R/R = (R_{RH} - R_{air})/R_{air}$) of the ZnO-MWCNT sensor while the relative humidity inside the chamber was varied by a controlled flow of moist air. The right hand y-axis represents the RH inside the chamber during the test.

The CH_4 sensor described here uses MWCNTs functionalized by metal oxide nanocrystals (MONCs) to sense methane. We used two well known MONCs, ZnO and SnO_2 that are widely used methane sensing materials and are inexpensive. ZnO and SnO_2 promote energetically favorable electron transport at the MO–MWCNT

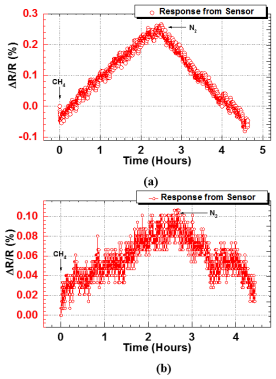

FIG. 8. (Color online) Relative resistance change of the SnO_2-MWCNT chemoresistor sensor while exposed to 10 ppm of CH_4 in dry air at (a) a lower RH (5%), and (b) a higher RH (70%) and was recovered by N_2. The circle symbol plot represents relative resistance change ($\Delta R/R = (R_{RH} - R_{air})/R_{air}$) of the chemoresistor sensor (left hand, y-axis) while the triangle symbol plot represents the RH inside the test chamber recorded by a commercial RH data logger (right hand, y-axis). Reproduced with permission from[26].

junction[6,20]. The work function of ZnO was reported to be almost 4.64 eV[43] or 5.2 eV[44], while SnO_2 has a work function of 4.7 eV[6]. The work functions of these MONCs are almost equal to the work function of MWCNTs (4.7-4.9 eV)[6,45]. Therefore, the Schottky barrier height at the MONC-MWCNT junction is low, facilitating electron transfer between MWCNTs and MONCs. The low Schottky barrier improves the overall sensitivity of the sensor (i.e high $\Delta R/R$ at low ppm), making the hybrid MONC-MWCNT system a potentially superior sensing element to either of its constituent components[6].

Table II compares the performance of our sensor with other published CNT CH_4 sensor. Note that although the sensor presented in[46] shows an equivalent performance to our sensors, it used wet chemically treated SWCNTs. Wet chemical treatment may be undesirable in CNT sensor fabrication as it is well known that acid treatments used in wet chemistry can considerably reduce the mechanical and electric performance of the tubes by introducing large numbers of defects[21], which might limit its reproducibility and reliability, as well as increase the cost of the sensor. Wet chemistry also involves additional steps, such as dissolution, sonication, mixing, and drying, which often causes undesirable agglomeration of treated CNTs.

IV. CONCLUSION

In summary, O_2 plasma activation has a stronger impact than UVO activation on enhancing the MONC functionalization of MWCNTs and thus on the response of the chemoresistive sensors to 10 ppm CH_4 in air. The strong relative resistance change in presence of 10 ppm of CH_4 at room temperature is a consequence of: (a) strong electron transfer to the MONCs from CH_4 molecules, (b) energetically favorable electron transport at the MONC-MWCNT junction, and (c) enhanced affinity of the dry surface activated MWCNT to MONCs as a result of formation of active chemical groups. The O_2 plasma and UVO-based activation processes give rise to COOH, C=O, and C-OH functional groups on the MWCNT surface, hence enhance the nucleation and bonding of MONCs with the MWCNT. These treatments produce strong reversible relative resistance change of the chemoresistors under iterative exposure to 10 ppm CH_4 in air and relatively reduced response to lower concentrations. The response varies with RH, with a lower response at higher RH as well as a lower detection limit. At low RH the detection limit is between 2 and 5 ppm.

ACKNOWLEDGMENTS

Use of the Center for Nanoscale Materials and Advanced Photon Source, Office of Science user facilities, was supported by the U. S. Department of Energy, Office of Science, Office of Basic Energy Sciences, under Contract No. DE-AC02-06CH11357. The US Environmental Protection Agency, through its Office of Research and Development, collaborated in the research described here. It has been subjected to Agency review and approved for publication. We would like to thank Scienta Omicron for loan of the Argus electron energy analyzer.

[1] Overview of greenhouse gases. `http://epa.gov/climatechange/ghgemissions/gases/ch4.html`. Accessed: 2 September 2015.
[2] D. Barrecaa, D. Bekermannb, E. Cominic, A. Devib, R. Fischerb, A. Gasparottod, C. Maccatod, G. Sberveglieric, E. Tondellod, Sens. Actuator B **149**, 1 (2010).
[3] P. Fau, M. Sauvan, S. Trautweiler, C. Nayral, L. Erades, A. Maisonnat, and B. Chaudret. Sens. Actuator B **78**, 83 (2001).
[4] T. Waitz, T. Wagner, T. Sauerwald, C.-D. Kohl, and M. Tiemann, Adv. Funct. Mater. **19**, 653 (2009).
[5] Y. Lu, J. Li, J. Han, H.-T. Ng, C. Binder, C. Partridge, and M. Meyyappan, Chem. Phys. Lett. **391**, 344 (2004).
[6] G. Lu, L. E. Ocola, and J. Chen, Adv. Mater. **21**, 2487 (2009).
[7] P. Qi, O. Vermesh, M. Grecu, A. Javey, Q. Wang, H. Dai, S. Peng, and K. Cho, Nano Lett. **3**, 347 (2003).
[8] C. Staii, A. T. Johnson, M. Chen, and A. Gelperin, Nano Lett. **5**, 1774 (2005).
[9] A. Felten, C. Bittencourt, J.-J. Pireaux, G. V. Lier, and J.-C. Charlier, J. Appl. Phys. **98**, 074308 (2005).
[10] Z. N. Utegulov, D. B. Mast, P. He, D. Shi, and R. F. Gilland, J. Appl. Phys. **97**, 104324 (2005).
[11] D.-Q. Yang and E. Sacher, J. Phys. Chem. C **112**, 4075 (2008).
[12] E.H. Espinosa, R. Ionescu, C. Bittencourt, A. Felten, R. Erni, G. Van Tendeloo, J.-J. Pireaux, and E. Llobet, Thin solid films **515**, 8322 (2007).
[13] P. Kar, and A. Choudhury, Sens. Actuators B **183**, 25 (2013).
[14] Z. Li, J. Li, X. Wu, S. Shuang, C. Dong, and M. M. F. Choi, Sens. Actuator B **139**, 453 (2009).
[15] Y. Li, H. Wang, Y. Chen, and M. Yang, Sens. Actuator B **132**, 155 (2008).
[16] K.E. Aasmundtveit, B.Q. Ta, A.V. Ngo, O. Nilsen, and N. Hoivik. *2014 IEEE 14th International Conference on Nanotechnology (IEEE-NANO)* (IEEE, 2014).

TABLE II. Comparison of CNT chemoresistor sensors

Material	LDL	Operating Temperature	Interference Gases
Pd-SWCNT[5]	15 ppm	Room Temperature (R.T.)	Not Mentioned (N.M.)
Pd-MWCNT[14]	3 vol %	R.T.	H_2, NH_3
Pd-MWCNT[11]	2 vol	R.T.	N.M.
Carbon Nanofiber[47]	500 ppm	R.T.	N.M.
Pt-CNT, Ru-CNT, Ag-CNT[48]	0.7 vol %	150 °C	CO_2, CO, NO_2, NH_3
SWCNT (wet chemical treated)[46]	2 ppm	R.T.	CO, SO_2, NH_3
ZnO-MWCNT, SnO_2-MWCNT (This work)	2 ppm	R.T.	H_2O

[17]S. Boukhalfa, K. Evanoff, and G. Yushin, Energy Environ. Sci. **5**, 6872 (2012).
[18]M.-G. Willinger, G. Neri, E. Rauwel, A. Bonavita, G. Micali, and N. Pinna,, Nano Lett. **8**, 4201 (2008).
[19]S. Heinze, J. Tersoff, R. Martel, V. Derycke, J. Appenzeller, P. Avouris, Phys. Rev. Lett. **89**, 106801 (2002).
[20]H. Zhang, N. Du, B. Chen, D. Li, and D. Yang, Sci. Adv. Mater. **1**, 13 (2009).
[21]A. Zamudio, A.L. Elías, J.A. Rodríguez-Manzo, F. López-Urías, G. Rodríguez-Gattorno, F. Lupo, M. Rühle, D.J. Smith, H. Terrones, D. Díaz, et al. Small **2**, 346 (2006).
[22]E. Najafi, J.-Y. Kim, S.-H. Han, and K. Shin, Colloid Surf. A **284**, 373 (2006).
[23]A. Ogino X. Wang C. Chen, B. Liang and M. Nagatsu. J. Phys. Chem. C **113**, 7659 (2009).
[24]R. Larciprete, S. Gardonio, L. Petaccia, and S. Lizzit, Carbon **47**, 2579 (2009).
[25]M. T. Humayun, R. Divan, L. Stan, A. Gupta, D. Rosenmann, L. Gundel, P. A. Solomon, and I. Paprotny, J. Vac. Sci. Technol. B **33**, 06FF01 (2015).
[26]M. T. Humayun, R. Divan, Y. Liu, L. Gundel, P. A. Solomon, and I. Paprotny. J. Vac. Sci. Technol. A **34**, 01A131-1 (2016).
[27]A. Ganguly, S. Sharma, P. Papakonstantinou, and J. Hamilton, J. Phys. Chem. C **115**, 17009 (2011).
[28]P.-L. Girard-Lauriault, René Illgen, J.-C. Ruiz, M. R. Wertheimer, and W. E. S. Unger, Appl. Surf. Sci. **258**, 8448 (2012).
[29]U. Zielke, K. J. Hüttinger, W. P. Hoffman, Carbon **34**, 983 (1996).
[30]P. Bindu, P. and S. Thomas, J. Theor. Appl. Phys. **8**, 123 (2014).
[31]R. Cuscó, E. Alarcón-Lladó, J. Ibanez, L. Artús, J. Jiménez, B. Wang, and M.J. Callahan, Phys. Rev. B **16**, 165202 (2007).
[32]X. Li, C. Li, Y. Zhang, D. P. Chu, W. I. Milne, and H. J. Fan, Nano. Res. Lett. **5**, 1836 (2010).
[33]E. F. Antunes, A. O. Lobo, E. J. Corat, and V. J. Trava-Airoldi, Carbon **45**, 913 (2007).
[34]M. T. Humayun, R. Divan, L. Stan, D. Rosenmann, D. Gosztola, L. Gundel, P. A. Solomon, and I. Paprotny. IEEE Sens. J. **16**, 8692 (2016).
[35]RV Gelamo, FP Rouxinol, C Verissimo, AR Vaz, MA Bica de Moraes, and SA Moshkalev. Chem. Phys. Lett. **482**, 302 (2009).
[36]W.-S. Cho, S.-I. Moon, Y.-D. Lee, Y.-H. Lee, J.-H. Park, and B. K. Ju. IEEE Elec. Dev. Lett. **26**, 498 (2005).
[37]J. Zhang, X. Liu, G. Neri, N. Pinna, Adv. Mater., **28**, 795 (2016).
[38]*Acc. of Chem. Res.*, H. Dai(12), Acc. of Chem. Res. **35**, 1035 (2002).
[39]O. K. Varghese, P. D. Kichambre, D. Gong, K. G. Ong, E. C. Dickey, and C. A. Grimes, Sens. Actuator B **81**, 32 (2001).
[40]P. S. Na, H. Kim, H.-M. So, K.-J. Kong, H. Chang, B. H. Ryu, Y. Choi, J.-O. Lee, B.-K. Kim, J.-J. Kim, et al. (9), App. Phys. Lett. **87**, 093101 (2005).
[41]K. G. Ong, K. Zeng, and C. A. Grimes, IEEE Sens. J. **2**, 82 (2002).
[42]J. Li J. W. Han, B. Kim and M. Meyyappan. J. Phys. Chem. C **116**, 22094 (2012).
[43]H. Moormann, D. Kohl, and G. Heiland, Surf. Sci. **80**, 261 (1979).
[44]X. Bai, E. G. Wang, P. Gao, and Z. L. Wang, Nano Lett. **3**, 1147 (2003).
[45]M. Shiraishi and M. Ata, Carbon **39**, 1913 (2001).
[46]A. Hannon, Y. Lu, J. Li, and M. Meyyappan, Sensors **16**, 349 (2016).
[47]R. K. Roy, M. P. Chowdhury, and A. K. Pal, Vacuum **77**, 223(2005).
[48]M. Penza, R. Rossi, M. Alvisi, and E. Serra, Nanotechnology **21**, 105501 (2010).